Magnetophotonic Response of Three-Dimensional Opals

José Manuel Caicedo,[†] Oana Pascu,[†] Martín López-García,[‡] Víctor Canalejas,[‡] Álvaro Blanco,[‡] Cefe López,[‡] Josep Fontcuberta,[†] Anna Roig,[†,*] and Gervasi Herranz[†,*]

[†]Institut de Ciència de Materials de Barcelona (ICMAB-CSIC), Campus UAB, E08193, Bellaterra, Spain and [‡]Instituto de Ciencia de Materiales de Madrid (ICMM-CSIC), Calle Sor Juana Inés de la Cruz 3, Madrid 28049, Spain

ABSTRACT Three-dimensional magnetophotonic crystals (3D-MPCs) are being postulated as appropriate platforms to tailor the magneto-optical spectral response of magnetic materials and to incorporate this functionality in a new generation of optical devices. By infiltrating self-assembled inverse opal structures with monodisperse nickel nanoparticles we have fabricated 3D-MPCs that show a sizable enhancement of the magneto-optical signal at frequencies around the stop-band edges of the photonic crystals. We have established a proper methodology to disentangle the intrinsic magneto-optical spectra from the nonmagnetic optical activity of the 3D-MPCs. The results of the optical and magneto-optical characterization are consistent with a homogeneous magnetic infiltration of the opal structure that gives rise to both a red-shift of the optical bandgap and a modification of the magneto-optical spectral response due to photonic bandgap effects. The results of our investigation demonstrate the potential of 3D-MPCs fabricated following the approach outlined here and offer opportunities to adapt the magneto-optical spectral response at optical frequencies by appropriate design of the opal structure or magnetic field strength.

KEYWORDS: photonic crystals · magnetic nanoparticles · magneto-optic enhancers · optical activity

Photonic crystals are materials in which the permittivity is periodically modulated on the scale of the optical wavelength, giving rise to a deep modification of the spectral optical response.[1−3] The addition of a magnetic component into these structures, the so-called magnetophotonic crystals (MPCs), has two main interesting effects. On one hand, it breaks time inversion symmetry, allowing nonreciprocal effects in light propagation.[4,5] On the other hand, light is slowed at frequencies of the photonic band edges, strongly increasing the light−matter interaction and enhancing the magneto-optical response.[6−8] The possibility of controlling the light propagation and modifying the magneto-optical spectral response by judicious material design makes the MPCs a very suitable platform for the development of a new generation of fast and compact isolators for optical data transmission and integrated optics.[9]

Along this line it has been demonstrated that the magneto-optical response of one- (1D) and two-dimensional (2D) MPCs is significantly enhanced at band edge frequencies.[10,11] This remarkable result has prompted the investigation of 3D-MPCs in which the periodicity in the three directions could lead to a complete photonic bandgap in the optical region, with an added functionality.[10,12,13] Nevertheless, the achievement of high-quality 3D-MPCs is much more complex and, therefore, the attainment of an optimal (magneto-) optical response—comparable at least to that of 1D-MPCs—remains a challenging issue.[14,15] Early reports on the magneto-optical characterization of 3D-MPCs has revealed some features around the photonic crystal stop-band that have been interpreted generally as a moderate increase of the magneto-optical activity around those frequencies.[16−18] However, little attention has been paid to the eventual occurrence of optical activity in 3D-MPC opals due to their structure and its relevance with respect to the intrinsic magneto-optical properties. Promising results were earlier reported on 3D photonic crystals impregnated with a Faraday-active transparent liquid.[11,19] Here we present the magnetophotonic response of 3D opals infiltrated with Ni nanoparticles. By exploiting newly developed methodologies to disentangle their intrinsic magneto-optical response from other sources of optical activity, we find a strong modification of the spectral response especially prominent near the photonic band edges.

RESULTS AND DISCUSSION

Al_2O_3 Inverse Opals Infiltrated with Ni Nanoparticles. The 3D-MPCs systems studied consist of Al_2O_3 inverse opals infiltrated with monodisperse Ni nanoparticles. For that purpose, two sets of 8 and 15 nm spherical and surfactant-stabilized Ni nanoparticles with good polydispersity of 12% (8 nm (Figure 1a and b)) and 10% (15 nm, data not shown) were synthesized by organometallic thermal decomposition method.[20] The two sets of Ni particles were superparamagnetic at room temperature, as indicated by the zero field

* Address correspondence to gherranz@icmab.es, roig@icmab.es.

Received for review December 24, 2010 and accepted March 4, 2011.

Published online March 14, 2011
10.1021/nn1035872

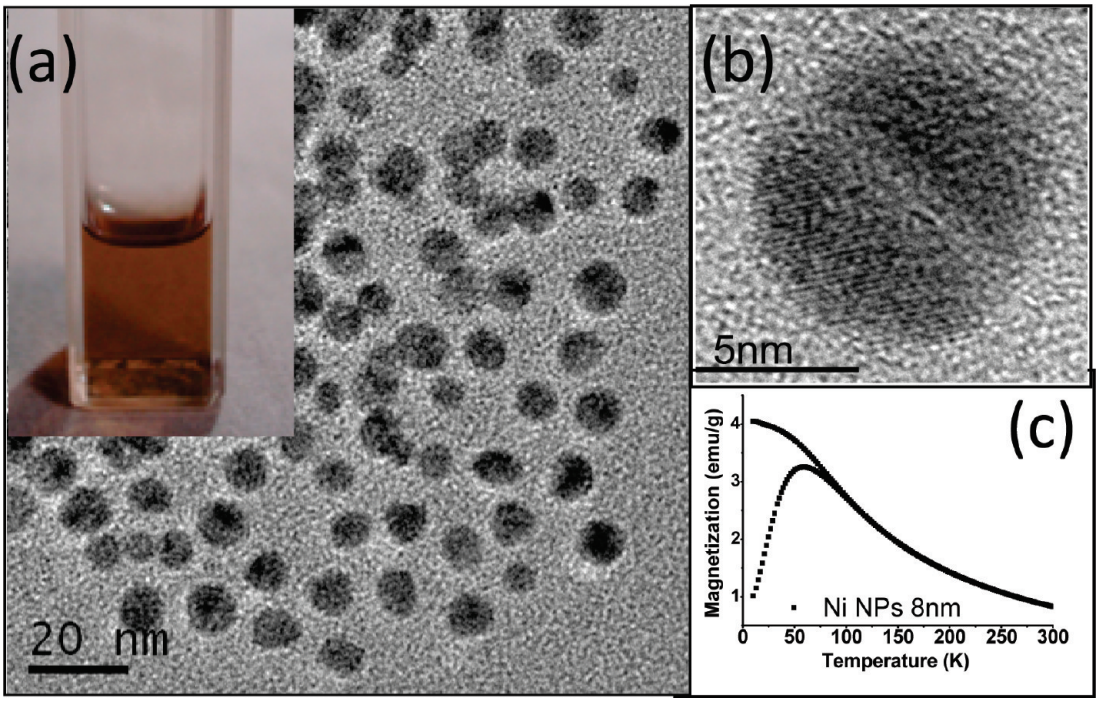

Figure 1. (a) Transmission electron microscopy (TEM) image of 8 nm Ni nanoparticles used for the infiltration and the corresponding stable colloidal dispersion image (inset). (b) High-resolution TEM image of a single 8 nm Ni nanoparticle. (c) Zero-field and field (50 Oe) magnetization *versus* temperature curves.

cooled−field cooled magnetization curve corresponding to 8 nm Ni nanoparticles (Figure 1c), with a blocking temperature (T_B) of 59 K. The saturation magnetization at 300 K was about 18 and 44 emu/g for 8 and 15 nm particles, respectively (not shown). Using these nanoparticles, the infiltration was done by dipping the inverse opals, described below, into stable colloidal dispersions (see the inset of Figure 1a) by using a step-motor-assisted dip-coating set up.[21,22]

The inverse opals were fabricated by self-assembly of polystyrene spheres (diameter 320 nm) onto hydrophilic glass substrates by standard vertical deposition.[23] Subsequently, conformal Al_2O_3 layers with controllable thickness were grown by atomic layer deposition (ALD) around the polystyrene spheres. To leave spherical voids in the Al_2O_3 structure, the original organic spheres were removed by dissolution with toluene. The resulting inverse opal was infiltrated with Ni nanoparticles as described above. Figure 2a shows a scanning electron microscope (SEM) overview picture of a typical Ni-infiltrated sample where the three-dimensional fcc compact stacking of the spherical opal units can be clearly appreciated. The same figure also allows discerning the hollow spheres that were broken during the sample preparation, revealing the inverse opal structure. Figure 2b shows an SEM image of the surface of the infiltrated opal. On one hand, Figure 2b noticeably reveals that Al_2O_3 forms a very uniform conformal coating on the polystyrene spheres. On the other hand, the tiny bright spots on the spherical surfaces—which are more visible in the zoomed image of the inset of Figure 2b—are the Ni nanoparticles.

SEM cross-sectional images of the 3D-MPCs (Figure 2c) were used to estimate the infiltration homogeneity across the depth of the opals and to determine the void (∼288 nm) and the connecting neck (∼100 nm) sizes, which are used for filling fraction calculations, $f_{air} = 0.87$ and $f_{Al2O3} = 0.13$, of air and alumina, respectively. The original contact points of the polystyrene spheres are clearly visible as the smaller windows in the inverse structure (Figure 2c). The zoom included in the inset of Figure 2c again unambiguously shows the presence of the Ni nanoparticles appearing as small bright spots across the image. This figure reveals also that the Al_2O_3 coating is homogeneous and has a thickness of about 15 nm.

Optical Transmittance: Stop-Band Red-Shift. The optical and magneto-optical properties of these 3D-MPCs were examined by performing optical transmittance (OT), circular dichroism (CD), and magnetic circular dichroism (MCD) spectroscopy experiments in the range of wavelengths $\lambda = 400-800$ nm. Although Faraday rotation and ellipticity were also recorded, their signals were largely masked by the large magneto-optical contribution of glass substrates, which made the analysis of the spectra quite difficult. On the contrary, the MCD signal, which in our configuration is proportional to the Faraday ellipticity,[24] was much stronger and was used to track the photonic effects on the magneto-optical spectra. The OT spectra were taken at normal incidence and allowed us to measure the stop-band frequencies of the MPCs. The CD and MCD data were obtained by using a lock-in amplified detection of the light transmitted through the samples using a photoelastic

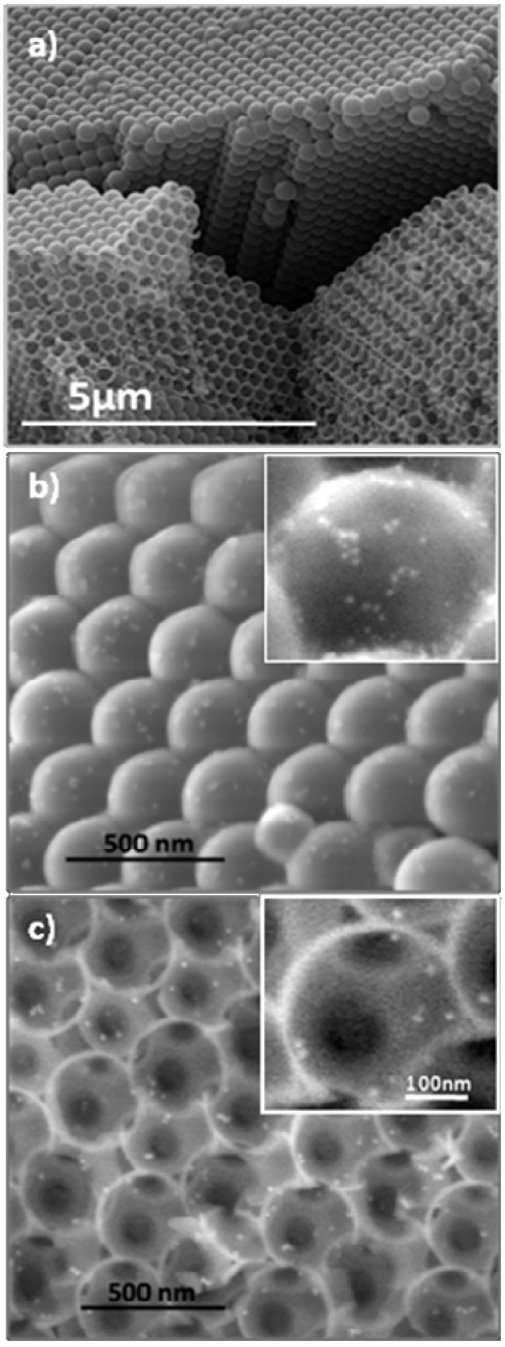

Figure 2. Scanning electron microscopy images of the opal after infiltration with 8 nm Ni nanoparticles: (a) overview, (b) surface, and (c) cross-section.

modulator.[20,25,26] In our setup configuration, the first harmonic of the detector signal is proportional to the dichroic (CD or MCD) signal $(I_{RCP} - I_{LCP})/(I_{RCP} + I_{LCP})$, where I_{RCP} and I_{LCP} are the right and left circularly polarized light transmitted through the 3D-MPCs, respectively. We stress that this setup allows the measurement of the optical and magneto-optical spectral response at exactly the same place on the crystals, with a light probe spot size of ~2 mm.[27]

We first performed OT experiments to determine the stop-band frequencies of the crystals. Figure 3 (left axis) shows the OT for the blank non-infiltrated opal (solid squares) as well as the opals infiltrated with 15 and 8 nm nanoparticle (solid triangles). We note that in Figure 3 the OT and MCD spectra are given in arbitrary units and have been shifted in order to facilitate their visual inspection. This data treatment, however, does not alter at all the conclusions of the combined analysis of the OT and MCD spectral responses discussed below. We observe in Figure 3 that the blank opal exhibits a stop band centered at $\lambda_B \approx 537$ nm, whereas after the infiltration with the Ni nanoparticles the stop band experiences a red-shift. This effect is very weak for the opal infiltrated with 15 nm nanoparticles, whereas it is substantial (~18 nm shift) for the opals infiltrated with 8 nm nanoparticles. The magnitude of the stop-band red-shift is directly related to the degree of the opal infiltration. To quantify this parameter, we calculated the effective refractive index (n_{eff}) of material before and after infiltration, from the experimental λ_B red-shift using the Bragg law for a fcc closed packed structure:[28]

$$\lambda_B = 2(2/3)^{1/2} D n_{eff} \quad (1)$$

where D is the sphere diameter of the photonic crystal (D = 316.8 nm in our case, which is obtained from the addition of the void diameter (288 nm) plus twice the Al_2O_3 shell thickness). From eq 1 we obtained n_{eff} = 1.039 for the original opal and n_{eff} = 1.073 and 1.044 for the opals infiltrated with Ni nanoparticles of 8 and 15 nm, respectively. From these values we could extract the volume fractions f_{Ni} of the infiltrated magnetic nanoparticles by using well-known effective medium approximations, *i.e.*, the Maxwell−Garnett equation[29]

$$\frac{n_{eff}^2 - 1}{n_{eff}^2 + 2} = f_{Ni}\frac{n_{Ni}^2 - 1}{n_{Ni}^2 + 2} + f_{Al_2O_3}\frac{n_{Al_2O_3}^2 - 1}{n_{Al_2O_3}^2 + 2} + f_{air}\frac{n_{air}^2 - 1}{n_{air}^2 + 2} \quad (2)$$

and Bruggeman equation[30]

$$0 = f_{Ni}\frac{n_{Ni}^2 - n_{eff}^2}{n_{Ni}^2 + 2n_{eff}^2} + f_{Al_2O_3}\frac{n_{Al_2O_3}^2 - n_{eff}^2}{n_{Al_2O_3}^2 + 2n_{eff}^2} + f_{air}\frac{n_{air}^2 - n_{eff}^2}{n_{air}^2 + 2n_{eff}^2} \quad (3)$$

where we also used the refractive indices of air (n_{air} = 1) and bulk Ni (n_{Ni} = 1.78). Using the f_{air} and the f_{Al2O3} values described above and the observed red-shift of the gap, the effective filling fraction of Ni has been determined. These estimates were virtually the same for both approaches, eq 2 and eq 3, and yielded $f_{Ni\text{-}15\,nm} \approx 1.1-1.3\%$ and $f_{Ni\text{-}8\,nm} \approx 9\%$ for the 3D-MPCs infiltrated with 15 and 8 nm nanoparticles, respectively. The smaller infiltration observed when using the 15 nm nanoparticles is likely related to the fact that when larger particles or higher concentrations are used, some blocking of the connecting necks of the opal takes place. Indeed, smaller filling fractions are also obtained when using 8 nm Ni nanoparticle dispersions of high enough concentrations (>10^{-3} M =

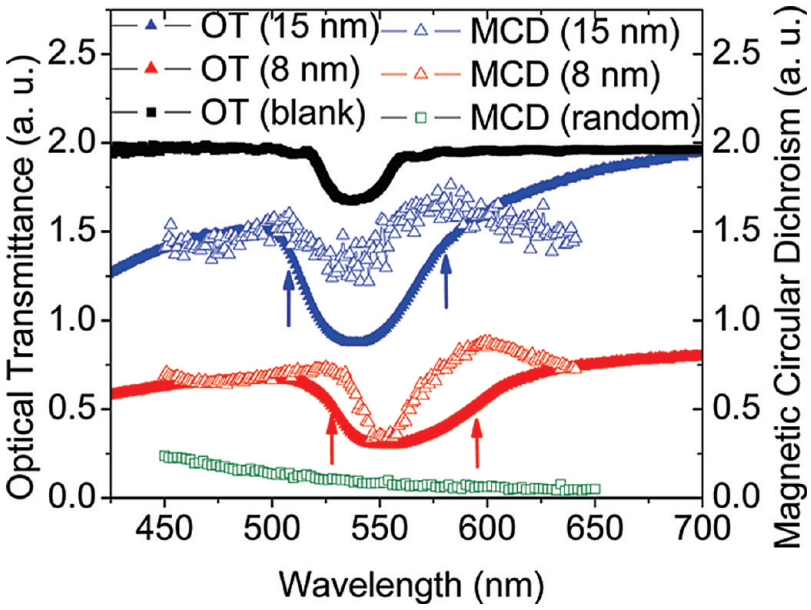

Figure 3. Optical transmittance (OT) of a non-infiltrated opal (blank) and opals infiltrated with 15 and 8 nm Ni nanoparticles. The figure also shows the magnetic circular dichroism (MCD) spectra of opals infiltrated with nanoparticles as well as the MCD spectra of Ni nanoparticles distributed randomly on a glass substrate. The arrows indicate the location of the magneto-optical enhancement discussed in the text.

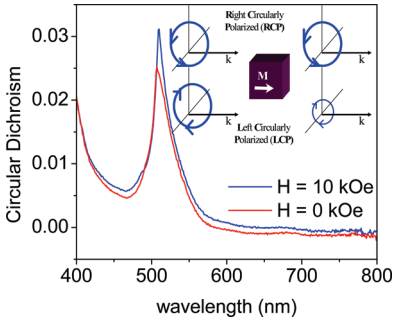

Figure 4. Circular dichroism (CD) spectra at zero field and at field H = 10 kOe of an inverse opal infiltrated with 8 nm Ni nanoparticles. The sketch in the inset shows the principle of the CD experiment.

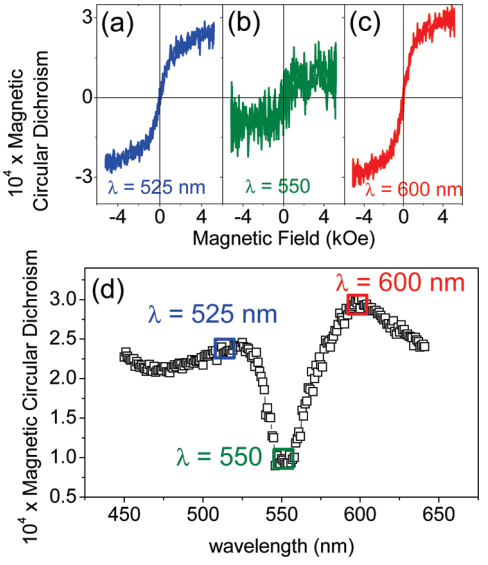

Figure 5. Magnetic circular dichroism (MCD) spectrum of an inverse opal infiltrated with 8 nm Ni nanoparticles is shown in (d). The data are obtained from the maximum amplitude of the full MCD hysteresis loops (see panels (a)−(c) for these loops at three selected wavelengths).

0.1 mg Ni NPs/mL solvent). Thus, optimal infiltration of 3D-MPCs requires small enough nanoparticle size and concentrations.

Magneto-optical Characterization: Band-Edge Enhancement. Once the structural quality of the photonic crystals and the efficiency of the infiltration with the magnetic nanoparticles have been assessed, we turn now to the investigation of their functional optical and magneto-optical properties. Following the commonly used approach,[31] we performed CD experiments by recording the intensity of the light transmitted though the opals (see inset of Figure 4) while sweeping the wavelengths in the absence of any magnetic field. For nonoptically active systems a null CD signal should be expected, but due to their particular compact fcc periodic structure, photonic crystals can indeed exhibit a significant CD near the stop-band frequencies, especially at off-normal incidence.[32,33] Here we show that this effect can be quite large even at normal incidence. Indeed, we see in Figure 4 that the CD spectrum of the opal infiltrated with 8 nm Ni nanoparticles is significantly large around the stop band. The application of a field of H = 10 kOe (well above the saturation field on the Ni nanoparticles) induces only an additional moderate increase of around 30% of the CD response. Thus, much of the optical activity of these 3D-MPCs has a nonmagnetic origin; it results from the geometry of the opal structure, and thus this technique does not allow

disentangling the distinct contributions to the optical activity. We used then a proper strategy in order to determine the intrinsic magneto-optical response of the crystals. For that purpose, and in order to have the complete information on their magneto-optical properties, we recorded the whole series of full hysteresis MCD loops of the 3D-MPCs with 1 nm step resolution, from λ = 400 nm to λ = 800 nm. The maximum amplitude of each hysteresis loop was then used to compute the MCD spectral response. As an illustration, we show in Figure 5d the MCD spectrum measured using this procedure, while Figure 5a−c displays the full hysteresis loops at selected wavelengths.

Once the protocol to measure the intrinsic MCD is established, we discuss now the magneto-optical spectral responses of the photonic crystals and their relation to their optical properties. Figure 3 depicts the OT (left axis) and MCD (right axis) spectra obtained at the same spot (diameter ~2 mm) in opals infiltrated with 8 and 15 nm nickel nanoparticles. Additionally, Figure 3 shows the MCD spectrum of a sample consisting of 8 nm nanoparticles distributed randomly on a glass substrate (empty squares). This spectrum is the reference of the MCD response of the Ni nanoparticles free of any crystal-induced photonic effect. Figure 3 immediately reveals a deep modification of the MCD spectra of the two 3D-MPCs with respect to that of the randomly distributed Ni nanoparticles. More specifically, a clear signature is observed of a magneto-optic enhancement in the form of two prominent shoulders in the MCD spectra around the two stop-band edge frequencies (which are indicated by arrows). Note that the frequency shift of the optical stop-band positions of the 3D-MPCs infiltrated with 8 and 15 nm nanoparticles is perfectly reproduced by the shift of the features of the MCD spectra induced by the photonic band effects. Therefore, the intensive modification of the magneto-optical response in close proximity of the band edge frequencies is in agreement with the theoretical predictions[11] and is a direct consequence of the strong increase of light matter interaction due to photonic band flattening and the resulting reduction of the light group velocity at band edge wavelengths.[34] Importantly such response can be tuned by the applied magnetic field. We finally point out that the photonic effect on magneto-optics in the 3D-MPC infiltrated with 8 nm is slightly larger than that of the one infiltrated with 15 nm nanoparticles (Figure 3), in agreement with the larger impregnation of Ni nanoparticles inside the crystal in that case compared to the former.

CONCLUSIONS

Our results show that an optimal infiltration of inverse opals with magnetic nanoparticles is a powerful strategy to customize the magneto-optical spectral response of magnetic materials. We have demonstrated that our approach can be exploited to generate a tailored magneto-optical response that is operative at least on the order of a few millimeters (the probe light spot size in our experiments). This shows that the structural order required to observe the photonic band induced effects is preserved in the same length scale, which makes still more appealing the approach here described for applications using lasers as light sources. We note that the superparamagnetic properties of the nanoparticles ensure an agile response of our system with the magnetic field, at variance with thin-layer infiltration, where a continuous layer would lead to hysteretic ferromagnetic behavior with more limited agility.

At the same time, a proper design of the geometrical parameters of the opal structure allows the determination at will of the range of wavelengths for which modification of the spectral response is desired. All these features are basic prerequisites for the development of novel optical devices in the field of optical data transmission and processing. As a possible further development in the field, one of the major advances would be to establish whether suitable strategies could be set to increase further the magnetic material content in the opal structures and analyze the impact of larger filling fraction factors in the optical spectral response.

MATERIALS AND METHODS

Fabrication of the Inverse Opals. The template material for the fabrication of the inverse opals was a self-assembled direct opal constituted of polystyrene spheres with 320 nm diameter. These direct opals were assembled by vertical deposition onto a hydrophilic glass substrate. Subsequently, an Al_2O_3 shell was infiltrated into this template by atomic layer deposition (ALD),[3] providing conformal layers around the polystyrene spheres of controllable thickness. In each ALD cycle around 1.8 Å was deposited. In our case, 80 cycles of ALD were used, forming an Al_2O_3 conformal layer thickness of around 15 nm (see also Figure 2c). Finally, the original polystyrene spheres were removed by dissolution in toluene, leaving spherical voids in the Al_2O_3 structure. The final inverse opal structure exhibited connection gate sizes of around 100 nm at the areas where initially the polystyrene spheres were in contact (Figure 2c). These connection gates provided the paths for the diffusion of Ni nanoparticles into the opals during the impregnation.

Synthesis of Ni Nanoparticles. Nickel nanoparticles were synthesized by a high-temperature solution-phase method adapting the procedures reported by Chen *et al.*[35] and Murray *et al.*[36] In a typical synthesis, 1 mmol (0.257 g) of $Ni(acac)_2$ was added to 7 mL of oleylamine, 2 mmol (0.63 mL) of oleic acid, and 1 mmol (0.45 mL) of trioctylphosphine, and the mixture was heated to 130 °C and stirred magnetically under a flow of high-purity argon. The mixture was kept for 20 min at 130 °C. Afterward, it was further heated up to 250 °C and maintained at this temperature for an

additional 30 min. After cooling to room temperature, the nanoparticles were precipitated by adding extra ethanol, followed by centrifugation. The resulting black precipitate can be redispersed in an organic nonpolar solvent. The precipitate was dried in an oven (at 70 °C) overnight and weighed. Finally, the as-synthesized nickel nanoparticles were kept in a hexane concentrated dispersion of known concentration.

Infiltration with Magnetic Nanoparticles. The infiltration was done by dipping the inverse opals into stable colloidal dispersions of two sets of Ni nanoparticles—with size 8 and 15 nm, respectively—and a concentration of 5×10^{-4} M (0.03 mg Ni/mL). The degree and homogeneity of the infiltration of the Ni nanoparticles into the inverse opals was controlled by the lifting-up speed (3.6 mm/h in our case), the number of infiltration cycles, and the size and concentration of the nanoparticles in the colloidal dispersion. As described in the main text, SEM cross-sectional pictures (Figure 2c) were instrumental to assess the homogeneity of the infiltration and the calculation of the filling factor fractions.

Circular Dichroism and Magnetic Circular Dichroism Spectroscopy. It was performed using a homemade experimental setup.[37,38] The sample reservoir was placed between the poles of an electromagnet. Light from a 150 W Xe arc lamp (ZolixTechnology) was dispersed by a monochromator (Zolix I-150), collimated, and then linearly polarized by the action of a Glan-Thompson prism, which is rotated 45° with respect to the modulator axis of a photoelastic modulator (PEM). After the PEM, the light was transmitted through the sample (with a typical light beam diameter of about ~2 mm) and then went toward a detector. The signal from this detector was brought to a lock-in amplifier synchronized to the frequency of the PEM retardation angle. It can be demonstrated that, in this setup configuration, one can measure the CD and MCD signals by inspection of the first harmonic of the detector signal.

Acknowledgment. We warmly acknowledge discussions on the subject with Antonio García Martín and Gaspar Armelles (CNM-CSIC). We acknowledge partial financial support from the CSIC CRIMAFOT (PIF 08-016), the Spanish Government (CONSOLIDER-Nanoselect-CSD2007-00041 and NanoLight.es-CSD20070046, MAT2008-06761-C03, MAT2009-08024, MAT2009-06885-E, MAT2009-07841, and FPI grant to J.M.C.), the Generalitat de Catalunya (2009SGR-376, 2009SGR-203, and FI grant to O.P.), the Comunidad de Madrid S-0505/ESP-0200, and the EC FP7 NoE Nanophotonics4Energy-248855.

REFERENCES AND NOTES

1. Yablonovitch, E. Inhibited Spontaneous Emission in Solid-Stated Physics and Electronics. *Phys. Rev. Lett.* **1987,** *58*, 2059–2062.
2. Johnson, S. G.; Joannopoulos, J. D. *Photonic Crystals: The Road from Theory to Practice*; Kluwer: Boston, 2001.
3. Galisteo-López, J. F.; Ibisate, M.; Sapienza, R.; Froufe-Pérez, L. S.; Blanco, A.; López C. Self-Assembled Photonic Structures. *Adv. Mater.* **2011**, *23*, 30−69.
4. Yablonovitch, E. Photonics: One Way Road for Light. *Nature.* **2009,** *461*, 744–745.
5. Wang, Z.; Chong, Y.; Joannopoulos, J. D.; Soljačić, M. Observation of Unidirectional Backscattering-Immune Topological Electromagnetic States. *Nature* **2009,** *461*, 772–775.
6. Takahashi, K.; Kawanishi, F.; Mito, S.; Takagi, H.; Shin, K. H.; Kim, J.; Lim, P. B.; Uchida, H.; Inoue, M. Study on Magnetophotonic Crystals for Use in Reflection-type Magneto-Optical Spatial Light Modulators. *J. Appl. Phys.* **2008,** *103*, 07B331–07B331-3.
7. Boriskina, J. V.; Erokhin, S. G.; Granovsky, A. B.; Vinogradov, A. P.; Inoue, M. Enhancement of the Magnetorefractive Effect in Magnetophotonic Crystals. *Phys. Solid State.* **2006,** *48*, 717–721.
8. Fedyanin, A. A.; Aktsipetrov, O. A.; Kobayashi, D.; Nishimura, K.; Uchida, H.; Inoue, M. Enhanced Faraday and Nonlinear Magneto-Optical Kerr Effects in Magnetophotonic Crystals. *J. Magn. Magn. Mater.* **2004,** *282*, 256–259.
9. Kato, H.; Matsushita, T.; Takayama, A.; Egawa, M.; Nishimura, K.; Inoue, M. Properties of One-Dimensional Magnetophotonic Crystals for Use in Optical Isolator Devices. *IEEE Trans. Magn.* **2002,** *38*, 3246–3248.
10. Inoue, M.; Fujikawa, R.; Baryshev, A.; Khanikaev, A.; Lim, P. B.; Uchida, H.; Aktsipetrov, O; Fedyanin, A.; Murzina, T.; Granovsky, A. Magnetophotonic Crystals. *J. Phys. D: Appl. Phys.* **2006,** *39*, R151–R161.
11. Zvezdin, A. K.; Belotelov, V. I. Magnetooptical Properties of Two Dimensional Photonic Crystals. *Eur. Phys. J. B* **2004,** *37*, 479–487.
12. Mekis, A.; Chen, J. C.; Kurland, I.; Fan, S.; Villeneuve, P.; Joannopoulos, J. D. High Transmission Through Sharp Bends in Photonic Crystal Waveguides. *Phys. Rev. Lett.* **1996,** *77*, 3787–3790.
13. Noda, S.; Tomoda, K.; Yamamoto, N.; Chutinan, A. Full Three-Dimensional Photonic Bandgap Crystals at Near-Infrared Wavelengths. *Science* **2000,** *289*, 604–606.
14. Liu, N.; Guo, H.; Fu, L.; Kaiser, S.; Schweizer, H.; Giessen, H. Three-Dimensional Photonic Metamaterials at Optical Frequencies. *Nat. Mater.* **2008,** *7*, 31–37.
15. Fang, M.; Volotinen, T. T.; Kulkarni, S. K.; Belova, L.; Rao, K. V. Effect of Embedding Fe_3O_4 Nanoparticles in Silica Spheres on the Optical Transmission Properties of Three-Dimensional Magnetic Photonic Crystals. *J. Appl. Phys.* **2010,** *108*, 103501–103501-6.
16. Pavlov, V. V.; Usachev, P. A.; Pisarev, R. V.; Kurdyukov, D. A.; Kaplan, S. F.; Kimel, A. V.; Kirilyuk, A.; Rasing, Th. Enhancement of Optical and Magneto-Optical Effects in Three-Dimensional Opal/Fe_3O_4 Magnetic Photonic Crystals. *Appl. Phys. Lett.* **2008,** *93*, 072502–072503.
17. Šimkiene, I.; Reza, A.; Kindurys, A.; Bukauskas, V.; Babonas, J.; Szymczak, R.; Aleshkevych, P.; Franckevicius, M.; Vaišnoras, R. Magnetooptics of Opal Crystals Modified by Cobalt Nanopartilcles. *Lith. J. Phys.* **2010,** *50*, 7–15.
18. Pavlov, V. V.; Usachev, P. A.; Pisarev, R. V.; Kurdyukov, D. A.; Kaplan, S. F.; Kimel, A. V.; Kirilyuk, A.; Rasing, Th. Optical Study of Three-Dimensional Magnetic Photonic Crystals Opal/Fe_3O_4. *J. Magn. Magn. Mater.* **2009,** *321*, 840–842.
19. Koerdt, C.; Rikken, G. L. J. A.; Petrov, E. P. Faraday Effect of Photonic Crystals. *Appl. Phys. Lett.* **2003,** *82*, 1538–1540.
20. Pascu, O.; Caicedo, J. M.; Fontcuberta, J.; Herranz, G.; Roig, A. Magneto-Optical Characterization of Colloidal Dispersions. Application to Nickel Nanoparticles. *Langmuir* **2010,** *26*), 12548–12552.
21. García, P. D.; Blanco, A.; Shavel, A.; Gaponik, N.; Eychmüller, A.; Rodríguez-González, B.; Liz-Marzán, L. M.; López, C. Quantum Dot Thin Layers Templated on ZnO Inverse Opals. *Adv. Mater.* **2006,** *18*, 2768–2772.
22. Caicedo, J. M.; Taboada, E.; Hrabovsky, D.; Lopez-Garcia, M.; Herranz, G.; Roig, A.; Blanco, A.; Lopez, C.; Fontcuberta, J. Facile Route to Magnetophotonic Crystals by Infiltration of 3D Inverse Opals with Magnetic Nanoparticles. *J. Magn. Magn. Mater.* **2010,** *322*, 1494–1496.
23. Jiang, P.; Bertone, J. F.; Hwang, K. S.; Colvin, V. L. Single-Crystal Colloidal Multilayers of Controlled Thickness. *Chem. Mater.* **1999,** *11*, 2132–2140.
24. Scott, G. B.; Lacklison, D. E.; Ralph, H. I.; Page, J. L. Magnetic Circular Dichroism and Faraday Rotation Spectra of $Y_3Fe_5O_{12}$. *Phys. Rev. B* **1975,** *12*, 2562–2571.
25. Stephens, P. J. Magnetic Circular Dichroism. *Annu. Rev. Phys. Chem.* **1974,** *25*, 201–232.
26. Caldwell, D.; Thorne, J. M.; Eyring, H. Magnetic Circular Dichroism. *Annu. Rev. Phys. Chem.* **1971,** *22*, 259–278.
27. By performing the optical and magneto-optical measurements on exactly the same location we avoided the effects associated with any eventual infiltration spatial inhomogeneities in the photonic crystals.
28. Minguez, H.; López, C.; Meseguer, F.; Blanco, A.; Vázquez, L.; Mayoral, R.; Ocaña, M.; Fornés, V.; Mifsud, A. Photonic Crystal Properties of Packed Submicrometric SiO_2 Spheres. *Appl. Phys. Lett.* **1997,** *71*), 1148–1150.
29. Garnett, J. C. M. Colours in Metal Glasses and in Metallic Films. *Philos. Trans. R. Soc. London, Ser. A* **1904,** *203*, 385–420.

30. Bruggeman, D. A. G. Berechnung verschiedener physikalischer Konstanten von heterogenen Substanzen. I. Dielektrizitätskonstanten und Leitfähigkeiten der Mischkörper aus Isotropen Substanzen. *Ann. Phys. (Leipzig)* **1935,** *416*, 636–664.
31. Mason, W. R. *Magnetic Circular Dichroism Spectroscopy*; Wiley: New York, 2007.
32. Gottardo, S.; Burresi, M.; Geobaldo, F.; Pallavidino, L.; Giorgis, F.; Wiersma, D. S. Self-Alignment of Liquid Crystals in Three-Dimensional Photonic Crystals. *Phys. Rev. E.* **2006,** *74*), 040702–040702-4.
33. Reza, A.; Simkiene, I.; Vaisnoras, R.; Lopez, C.; Golmayo, D.; Babonas, J. Optical Anisotropy of Synthetic Opals. *Photonics Nanostruct.* DOI: 10.1016/j.photonics.2010.10.003.
34. Galisteo-López, J.; Galli, M.; Patrini, M.; Balestreri, A.; Andreani, L.; López, C. Effective Refractive Index and Group Velocity Determination of Three-Dimensional Photonic Crystals by Means of White Light Interferometry. *Phys. Rev. B* **2006,** *73*, 125103–125103-9.
35. Chen, Y.; Peng, D. L.; Lin, D.; Luo, X. Preparation and Magnetic Properties of Nickel Nanoparticles via the Thermal Decomposition of Nickel Organometallic Precursor in Alkylamines. *Nanotechnology* **2007,** *18*, 505703–505708.
36. Murray, C. B.; Sun, S.; Doyle, H.; Betley, T. Colloidal Synthesis of Nanocrystals and Nanocrystals Superlatices. *IBM J. Res. Dev.* **2001,** 47–56.
37. Caicedo, J. M.; Dekker, M. C.; Dörr, K.; Fontcuberta, J.; Herranz, G. Strong Magnetorefractive and Quadratic Magneto-Optical Effects in $(Pr_{0.4}La_{0.6})_{0.7}Ca_{0.3}MnO_3$. *Phys. Rev. B* **2010,** *82*, 140410–140414.
38. Caicedo, J. M.; Arora, S. K.; Ramos, R.; Shvets, I. V.; Fontcuberta, J.; Herranz, G. Large Magnetorefractive Effect in Magnetite. *New J. Phys.* **2010,** *12*, 103023–103023-8.